Many Authors

JET Papers presented to the 11th Colloquium on UV and X-Ray Spectroscopy of Astrophysical and Laboratory Plasmas (Nagoya, Japan, 29 May- 2 June 1995)

JET Papers presented to the 11th Colloquium on UV and X-Ray Spectroscopy of Astrophysical and Laboratory Plasmas (Nagoya, Japan, 29 May- 2 June 1995)

Many Authors

JET-Joint Undertaking, Culham Science Centre, OX14 3EA, Abingdon, UK

JET Papers presented to the 11th Colloquium on
UV and X-Ray Spectroscopy of Astrophysical and Laboratory Plasmas
(Nagoya, Japan, 29 May – 2 June 1995)

Contents

Cl XV AND CL XVI IN THE JET AND COMPASS-D TOKAMAKS

I.H.Coffey [1], R.Barnsley[2] , F.P.Keenan[1], I.Melnick[3], P.McGinnity[1], M.G.O'Mullane[4] and N.J.Peacock

UKAEA-Goverment Division, (EURATOM/UKAEA Fusion Association) The Culham Laboratory, Abingdon, OXON, OX14 3DB, United Kingdom

[1] *Queens University, Belfast, BT7 1NN, Northern Ireland*
[2] *JET Joint Undertaking, Abingdon, OXON, OX14 3EA, United Kingdom*
[3] *University College London WC1E 6BT, England*
[4] *University College Cork, Ireland*

Abstract

Studies of the soft X-ray emission spectrum of He-like Cl XVI and its associated Li-like Cl XV satellites from the JET (Joint European Torus) and COMPASS-D tokamaks are reported. Observations are made of the emission from this intrinsic impurity species using the same high resolution ($\lambda/\delta\lambda \simeq 3000$) curved crystal spectrometer (CCS) with a CCD detector [1], enabling a comparison to be made of the effect of widely differing plasma conditions between the two devices. A range of diagnostic measurements are made from the observed spectral region: T_e and n_e and ionisation balance information from line ratio techniques, T_i and V_ϕ (toroidal plasma rotation) from doppler line width and wavelength shift measurements respectively and heat transport studies by simultaneous observation of T_e and T_i, in particular the electron-ion heat transfer rate.

1. Introduction

Spectroscopic measurements of He-like systems are often used for plasma diagnostics. In this report observations of the intrinsic He-like Cl XVI impurity spectrum from the JET and COMPASS-D tokamaks are compared, reflecting the widely differing plasma conditions between the two devices (see table 1) and showing the range of diagnostic capability appropriate to each device. Sample spectra from JET and COMPASS-D are shown in fig.1. In addition to the resonance line w, $(1s2p\,^1P_1 \rightarrow 1s^2\,^1S_0)$ the intercombination lines x and y $(1s2p\,^3P_{2,1} \rightarrow 1s^2\,^1S_0)$ and the forbidden line z $(1s2s\,^3S_1 \rightarrow 1s^2\,^1S_0)$, four satellite lines are visible: the dielectronic lines d_{13} $(1s2p3p\,^2D_{5/2} \rightarrow 1s^23p\,^2P_{3/2})$ and k $(1s2p^2\,^2D_{3/2} \rightarrow 1s^22p\,^2P_{1/2})$ and the inner-shell excitation q and r lines $(1s2s2p\,^2P_{3/2,1/2} \rightarrow 1s^22s\,^2S_{1/2})$. Also labelled is the j $(1s2p^2\,^2D_{5/2} \rightarrow 1s^22p\,^2P_{3/2})$

1

line which is blended with the z line and the $n \geq 3$ satellites on the long wavelength side of the resonance line.

Since there is a tendancy for the ion shells to radiate from the same region of the temperature profile irrespective of small changes in the temperature gradient and ion transport, the JET spectrum as illustrated is representative of most discharges. The relatively high satellite intensities are a feature of the lower temperature COMPASS-D plasmas (the highest temperature COMPASS-D spectra are similar to the JET spectrum shown). Of particular note is the appearance of a shoulder on the long wavelength side of the y line corresponding the nuclear spin allowed $1s2p\,^3P_0 \rightarrow 1s^2\,^1S_0$ transition. The wavelengths for this line are measured at $4.4688\text{\AA}$ and $4.4697\text{\AA}$ from COMPASS-D and JET respectively. These compare well with the calculated value of $4.4688\text{\AA}$ [2]. Due to the lower T_e in COMPASS-D the CL XVI spectra all emanate from the core region, a situation more conducive to spectroscopic plasma diagnostics.
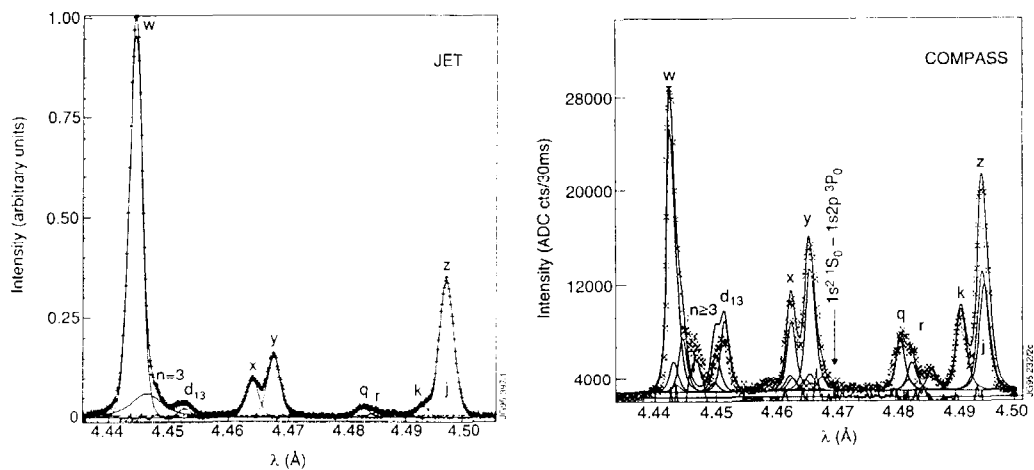
Fig. 1. *Curved Crystal Spectrum of Cl XVI from JET (left) and COMPASS-D (right).*

Table 1. Comparison of main parameters for the JET and COMPASS-D tokamaks

Parameter	JET	COMPASS-D
Major radius R (m)	2.96	0.557
Minor radius a (m)	1.25	0.232
Vertical radius b (m)	2.10	0.385
Toroidal magnetic field B_ϕ (T)	3.45	2.1
Plasma current I_P (MA)	7.0(max)	0.28
Electron Temperature T_e (KeV)	3.5 – 10.0	0.50 – 1.0
Electron Density $\overline{n_e}$ ($\times 10^{13}\text{cm}^{-3}$)	0.8 – 12	0.8 – 12
Pulse Duration (s)	25	0.4
NBI Power (MW)	20	–
ICRH power (MW)	20	–
ECRH power (MW)	–	2
LHCD power (MW)	3	0.6

2. Line Ratio Measurements

The main lines in the He-like isoelectronic sequence w, x, y and z may be used to infer the electron temperature sensitive ratio: $G = (x+y+z)/w$ which is density independent for JET and COMPASS-D conditions. (the electron density sensitive ratio $R = z/(x+y)$ is in its low density limit for both JET and COMPASS-D, ie. it only shows variation above $n_e \simeq 10^{14} \mathrm{cm}^{-3}$). The Li-like satellite lines can be used in conjunction with the w line to produce the diagnostic ratios: k/w and d_{13}/w which vary as $1/T_e$ and q/w which is dependent on the ionisation balance $N(Li)/N(He)$.
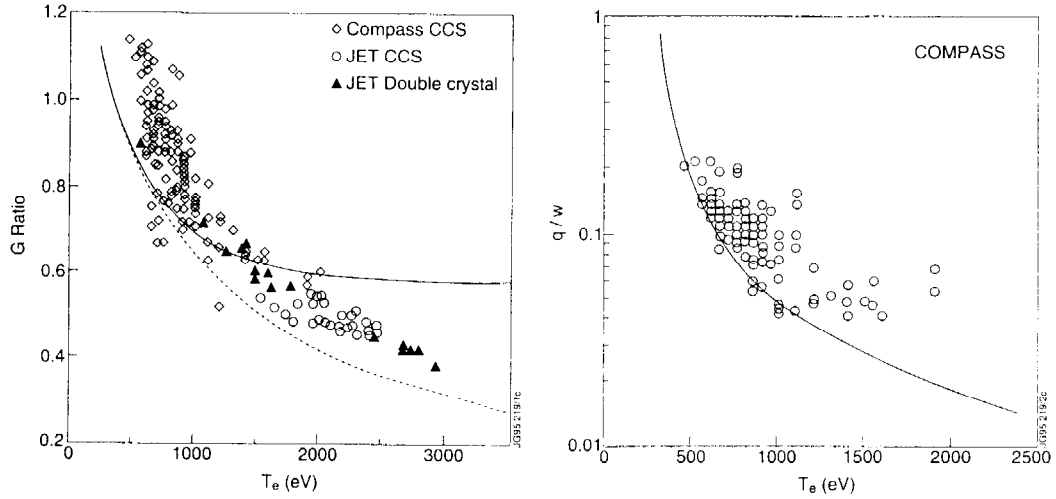

Fig. 2. *The theoretical emission ratio G (left) plotted as a function of T_e at an electron density of $n_e = 3.2 \times 10^{13} \mathrm{cm}^{-3}$, with dielectronic recombination included in (solid line) or excluded from (dashed line) the calculations. Experimental points from the JET (circles) and COMPASS-D (diamonds) tokamaks are shown and in addition JET results from a double crystal spectrometer (triangles)[3] are displayed to extend the T_e range. On the right the ratio q/w is plotted as a function of T_e. Equilibriun values for $N(Li)/N(He)$ have been used in the calculations. Experimental points from COMPASS-D are shown (circles).*

In fig.2 the experimental G ratios from JET and COMPASS-D are plotted against T_e in conjunction with theoretical ratios [3]. The k/w is used as a temperature measurement for the COMPASS-D ratios as the line components are well resolved and independent of ionisation balance. Non spectroscopic diagnostics provide $T_e(R)$ values for the JET data (in general the satellite lines from the higher temperature JET spectra are relatively too small to provide accurate T_e measurements).

Between approximately 800eV and 1500eV the ratio agrees with the coronal prediction. Below this temperature the triplet levels of the COMPASS-D ratios appear to have enhanced intensity above the coronal prediction. Possible explanations include: recombination (which is unlikely as it is not a cooling plasma and the $N(H)/N(He)$ ratio would be too low at these temperatures to have a significant effect) and inner-shell ionisation of the Li-like stage. A large proportion of the Li-like ions will be in the excited $1s^2 2p\,^2 P_{1/2,3/2}$ state [4], so both the ionising transitions $1s^2 2s\,^2 S_{1/2} \rightarrow 1s2s\,^3 S_1$ and $1s^2 2p\,^2 S_{3/2,1/2} \rightarrow 1s2p\,^3 P_{2,1}$ are possible. This would require an enhanced $N(Li)/N(He)$ ratio which would naturally occur with transport. Above 1500eV the measured ratios (predominately JET) fall below the coronal prediction. At these higher temperatures where, the Cl XVI emission shell will be off-axis, diffusion effects tend to lead to a reduction in $N(H)/N(He)$ from the equilibrium value with a corresponding lowering of the

measured ratio as a result of reduced recombination into the triplet states.

Fig.2 also shows the experimental q/w ratio from COMPASS-D. Again the k/w ratio is used to provide T_e values. This ratio is in general higher than the coronal model due to transport effects causing a higher N(Li)/N(He) ratio. This effect is larger at lower densities [5], thus at higher T_e where the n_e is lower (a COMPASS-D characteristic) there is a definite trend away from the coronal balance due to radial ion diffusion.

3. Doppler Measurements of T_i and V_ϕ

The ability to simultaneously measure core values T_e (from the k/w ratio) and T_i (from the linewidth) on a 10 - 15ms timescale allows an investigation of features of the heat transport, in particular the electron-ion heat transfer rate. Fig.4 shows the measured values of T_i against the corresponding T_e. The T_i measurements are compared with Artsimovich scaling [6]:

$$T_i = \frac{2.8 \times 10^{-6}}{A_i^{\frac{1}{2}}}(I_p B_\phi R^2 \overline{n_e})^{\frac{1}{3}}$$

where A_i is the deuterium (plasma fuel ion) mass. The measured values are generally lower but they do increase with the Artsimovich parameters. The electron temperatures for the equivalent shots have been added. At low n_e, T_e is high and T_i is low, as n_e increases, T_e decreases and T_i increases. This can be understood from power balance considerations. At low n_e the electron conduction is anomalous and fast. As n_e increases less power is lost through conduction and more is transferred to the ions. Coulomb collisions with the electrons are the only ion heating mechanism on COMPASS-D
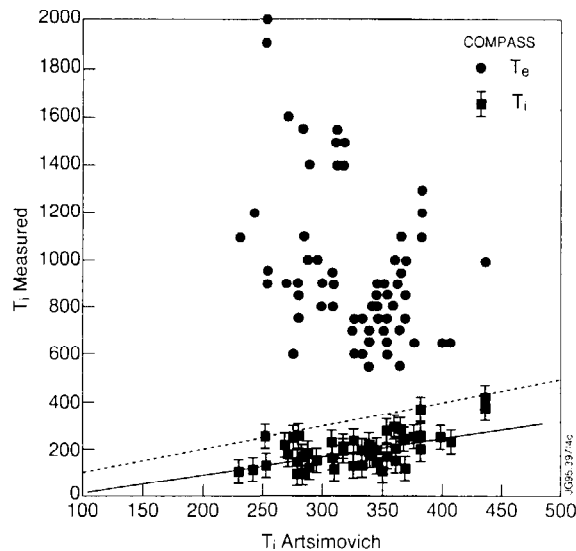

Fig. 3. *Electron and ion temperatures derived from the COMPASS-D Cl spectrum. The k/w ratio was used for T_e while line shapes of z were used for T_i. The lower group of points ($< 450eV$) refer to T_i while the upper group ($> 400eV$) refer to T_e. T_i scaling due to Artsimovich is shown broken, while the solid line is the best fit to the T_i data.*

Fig. 4. shows the changes observed in V_ϕ for JET and COMPASS-D respectively. For JET Neutral Beam Injection (NBI) heating results in a change of $\simeq$ 100kms^{-1} (in this example) by direct momentum transfer to the plasma. The reduction in the H_α signal at 55s signifies the beginning of an H-mode (high confinement regime). The rotation falls off slowly after the NBI period until the end of the H-mode when a step in V_ϕ is observed, after which V_ϕ falls off rapidly. Note the increase in the radial position of

4

maximum emissivity of the Cl XVI emitting shell with increasing central T_c during the heating period. For COMPASS-D, where there is no NBI, changes in V_ϕ of typically 20kms^{-1} in the ion drift direction are observed in the edge ions of B IV and in the core ions of Cl XVI as the plasma enters the H-mode. The H-mode signature is shown by the reduction in the H_α signal caused by a lessening in plasma wall interactions and edge recycling during this period. This momentum change in the bulk plasma is not well understood, but could be due to a combination of enhanced diamagnetic drifts and relaxation of viscous and frictional forces in the H-mode.
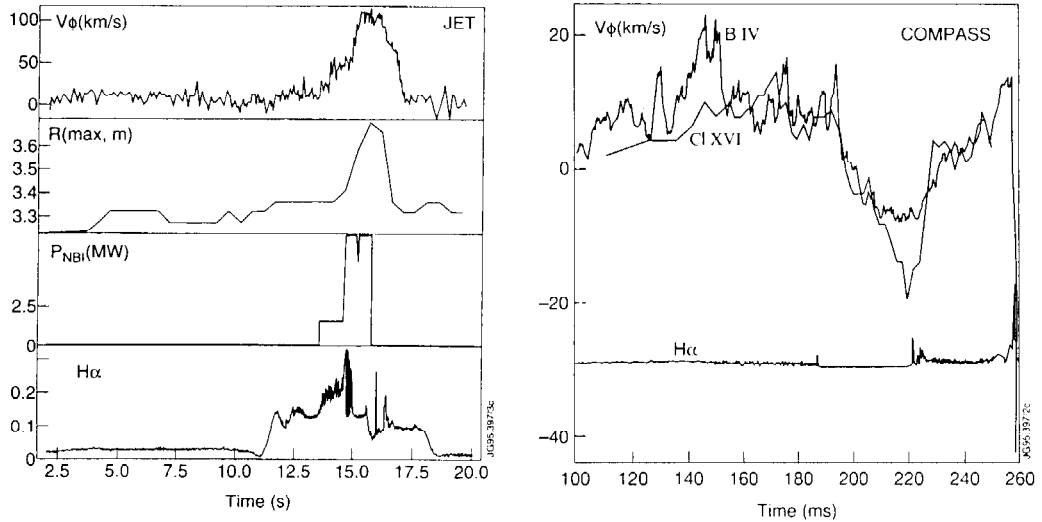

Fig. 4. V_ϕ measurements from JET (left) shown in conjunction with the calculated radial position of maximum Cl XVI emissivity (R_{max}, m), NBI injection power (MW) and the H_α emission. The V_ϕ measurements from COMPASS-D (right) are shown in conjunction with similar measurements from B IV at the plasma edge [7] and the H_α emission.

4. Conclusions

High resolution spectroscopic studies ($\lambda/\delta\lambda \simeq 3000$) of the intrinsic ClXVI system and its associated Cl XV satellites have produced a broad range of diagnostic information from a relatively narrow spectral region. Simultaneous easurements of T_e, T_i, ionisation balance, V_ϕ and electron-ion heat transfer can been made from the observed spectra. Such methods are not routinely used on the JET device, however they provide useful diagnostic information on COMPASS-D where the operating parameters are suited to such measurements.

5. References

1. Abbey, A.F. et al, Proc. 10th International Colloquium on UV and X-ray Spectroscopy, Berkeley, California. Cambridge University Press (1992)
2. Drake, G.W. Can.J.Phys., 66, 568 (1988)
3. Coffey, I.H. et al, Physica Scripta, 47, 169 (1993)
4. McWhirter, R.W.P., Plasma Radiation from Plasma Physics and Nuclear Fusion Research. (ed. Gill, R.D.) Academic Press (1981)
5. TFR group et al, Phys.Rev., A32, 2374 (1985)
6. Artsimovich, L.A., Nucl.Fusion, 12, 215 (1972)
7. Bamford, R.A., PhD Thesis, University of Essex (1994)

Ar XVII and Ar XVIII in the JET Tokamak

P.McGINNITY[1], R.BARNSLEY, I.H.COFFEY[1], F.P.KEENAN[1], M.G.O'MULLANE[2],
N.J.PEACOCK[2]
JET Joint Undertaking, Abingdon, OXON, OX14 3EA, UK
[1] *Queens University, Belfast, BT7 1NN, Northern Ireland*
[2] *UKAEA-Goverment Division, (EURATOM/UKAEA Fusion Association),*
Culham Laboratory, Abingdon, OXON, OX14 3DB, UK

1. Abstract

Observations of H-like Ar XVIII and He-like Ar XVII and its associated Li-like satellite spectra have been made on the JET tokamak. G, α and β intensity ratios have been derived from recently calculated atomic data and, after extensive transport modelling to account for diffusive effects in the plasma, compared with measured values. The measured G-ratio disagrees with the calculated ratio and with a previously published ratio and some possible reasons are given. The α and β ratios show the expected temperature and density sensitivity respectively.

2. Introduction

Argon was introduced into the JET plasma in two ways: by gas puffing in earlier pulses and by the use of an Ar frosted cryo-pump during He transport studies in more recent pulses. The following intensity ratios were measured: $G = (x + y + z)/w$, $\alpha = Ly_\alpha/w$ and $\beta = Ly_{\alpha_2}/Ly_{\alpha_1}$ where w, x, y and z are the main transitions to the $n = 2$ level in the He-like spectrum (labelled using the system of [3]) and ($Ly_{\alpha_{1,2}}$) are the fine structure Lyman lines from the $2p^2 P_{\frac{3}{2}}$ and $2p^2 P_{\frac{1}{2}}$ levels respectively.

Two spectrometers, a double crystal monochromator and a Bragg rotor instrument [1] were employed in the measurement of the argon spectra. Three distinct measurements were made: the He-like system was measured using both instruments, Ly_α using the double crystal and the Bragg rotor monitored the resonance lines from both ionisation stages. Examples of the measured spectra are shown in Fig.1. The spectra were fitted using a pseudo-Voigt routine, a convolution of Gaussian and Lorentian profiles. For most data the line shape was almost entirely Gaussian, being dominated by thermal broadening.
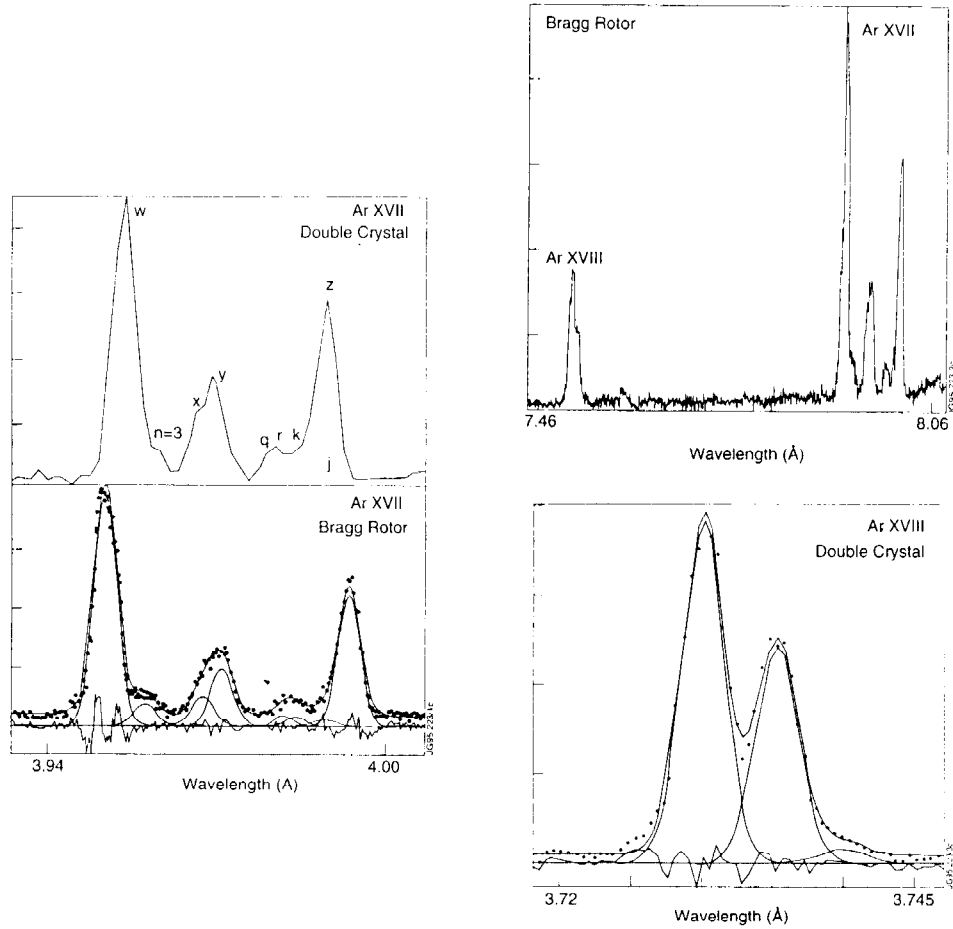
Fig. 1. (Left) Main $n = 2$ Ar XVII lines from the double crystal and Bragg rotor instruments respectively with associated Ar XVI dielectronic and inner shell satellites. (Top Right) High resolution double crystal Ar XVIII Ly_α line components and (Bottom Right) Bragg rotor spectrum scanning both the Ar XVIII Ly_α and Ar XVII n=2 lines in 2nd order.

Atomic data (electron excitation and dielectronic and radiative recombination rates, ionic level energies and Einstein A coefficients) were processed using the ADAS collisional radiative balance code [7] to derive level populations for a range of electron temperatures and densities. Transport modelling, via a transport code SANCO [4] which uses experimental radial density and temperature profiles as inputs, is employed to simulate JET transient plasma conditions and provide an ionisation balance which includes diffusive effects. Calculated level populations are coupled with the ionisation balance calculated from SANCO by a line emission code which provides emission profiles (integrated over temperature and density for the specific line-of-sight of the spectrometer), positions and values of maximum emissivity and calculated ratios.

3. He-like G-ratio

The G ratio is temperature sensitive but density independent as changes in n_e redistribute the populations of the upper triplet levels while the sum of the intercombination intensities remains constant for a given temperature.

Ar XVII measurements with the Bragg rotor were made by operating in repetitive scan mode using a PET(002) crystal $(2d = 8.742\text{Å})$ in second order with a wavelength resolution $\left(\frac{\lambda}{\delta\lambda}\right) \simeq 650$. The n=2 He-like system was also measured by the double crystal x-ray monochromator operating in survey mode with a Ge(111) crystal $(2d = 6.532\text{Å})$ covering a wavelength range from 3.75 to 4.20Å with a resolving power of $\simeq 550$.

A scaling factor for the ratio of the integrated line intensity to emission peak was used to reduce the G ratio to a single representative temperature at the radius of maximium emissivity, enabling experimental ratio to be plotted (Fig.2). The complete blending of the dielectronic satellite j with z was taken into account by deriving its intensity from the measured k intensity using an expression for dielectronic satellite intensities relative to the resonance intensity which is independent of n_e and ionisation balance but strongly dependent on T_e [2]. In general the experimental ratio is higher than that expected from calculations for ohmic, L and H-mode plasmas. The two coronal cases (with and without recombination from Ar XVIII included) are expected to be extreme values for JET. In the JET plasma, recombination is an important populating process but the emission shell occurs at temperatures higher than those expected from the coronal approximation due to diffusion.
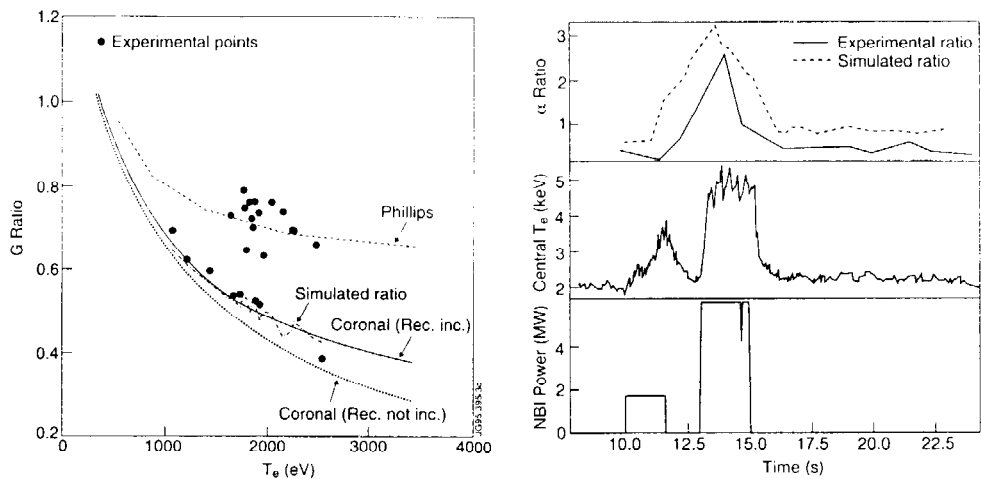

Fig. 2. (Left) The theoretical emission ratio G plotted as a function of electron temperature T_e for an electron density n_e in the range $1 - 10 \times 10^{13}cm^{-3}$, with dielectronic and radiative recombination included (solid line) and not included (dashed line) in the calculations. Also included are experimental values measured at JET, a theoretical G ratio calculated using an ionisation balance derived for JET plasma conditions at each experimental point and the calculated coronal G ratio of Phillips et al 1994 [5] for comparison.

Fig. 3. (Right) Measured (solid line) and calculated (dashed line) α-ratios as a function of time during a JET pulse (JPN 33314). The measured central electron temperature and total input neutral beam heating power for the same shot.

These results cast some doubt on the validity of the atomic data employed in the calculations, especially when compared to the G-ratio calculated by Phillips et al. The

electron collision excitation rates have been derived from interpolations of R-matrix calculations which have been thoroughly tested for other medium Z ions and have also been used by Phillips. Different methods of calculation of recombination rates have been employed and this is thought to be where the discrepancy arises.

There are two distinct regions in which the experimental points lie (Fig.2) All of the measured ratios from the Bragg rotor lie in the upper region but the double crystal values are spread over the two. This has been extensively investigated by varying transport parameters in the SANCO simulation, by checking for transient effects in the measured spectra due to the finite time taken by the spectrometers to scan the whole He-like system and by excluding other systematic errors. However, the reason is still unclear.

4. H-like to He-like resonance line intensity ratio

The α-ratio is temperature and H-like to He-like ionisation balance dependent due to the expression:

$$\frac{I_{Ly_\alpha}}{I_w} = \frac{N_H C_{Ly_\alpha}(T_e)}{N_{He} C_w(T_e)}$$

In this case the spectra were measured using the Bragg rotor in the same set-up as in the G-ratio measurement.

In this case the spectral separation of the lines meant that a sensitivity calibration of the PET cystal was required. The theoretical calibration of [7] was used. The calculations made using an ionisation balance from the SANCO code are consistently slightly smaller. This shift is within the uncertainties of the aforementioned calibration. It is clear, bearing in mind the time resolution of the measurements that the increase in the ratio corresponds to the increase in temperature due to NBI heating.

5. Fine Structure Intensity Ratio

$$\beta = \frac{I(1s^2 S_{\frac{1}{2}} - 2p^2 P_{\frac{1}{2}})}{I(1s^2 S_{\frac{1}{2}} - 2p^2 P_{\frac{3}{2}})}$$

The emission oscillator strengths are in a ratio of 2:1 for the $^2P_{\frac{3}{2}}$:^{2} $P_{\frac{1}{2}}$ levels of H-like ions, giving a statistical β-ratio of 0.5. However, at typical tokamak densities the probability of collisional de-excitation (by plasma fuel ions) of the $^2S_{\frac{1}{2}}$ electron population becomes larger than the transition proability for radiative decay by two photon emission. The $2s^2 S_{\frac{1}{2}}$ level is very close to the $2p^2 P_{\frac{1}{2}}$ level and therefore particle collisions would be expected to preferentially populate this state leading to an observed increase in the β-ratio from 0.5.

Double crystal measurements of the Ar XVIII Ly_α components were made by operating in repetitive scan mode over a wavelength range of 3.70 to 3.82Å again with the Ge(111) crystal with a fine collimator giving a resolving power of $\simeq$ 5000. For the three shots analysed, Ar was puffed at 13s but it was not until neutral beam heating was switched on at 16s and the density rose, that a measurable Ar signal was detected. As the central n_e rises from $\sim 2 \times 10^{13} cm^{-3}$ at 16s to $\sim 5.5 \times 10^{13} cm^{-3}$ at 19s, a corresponding rise is observed in the averaged β-ratio of $\sim$ 10%. The discrepancy between the calculated (neglecting heavy particle excitation) and measured ratios increases with density as does the expectation of population transfer to the lower level by heavy particle collisions.
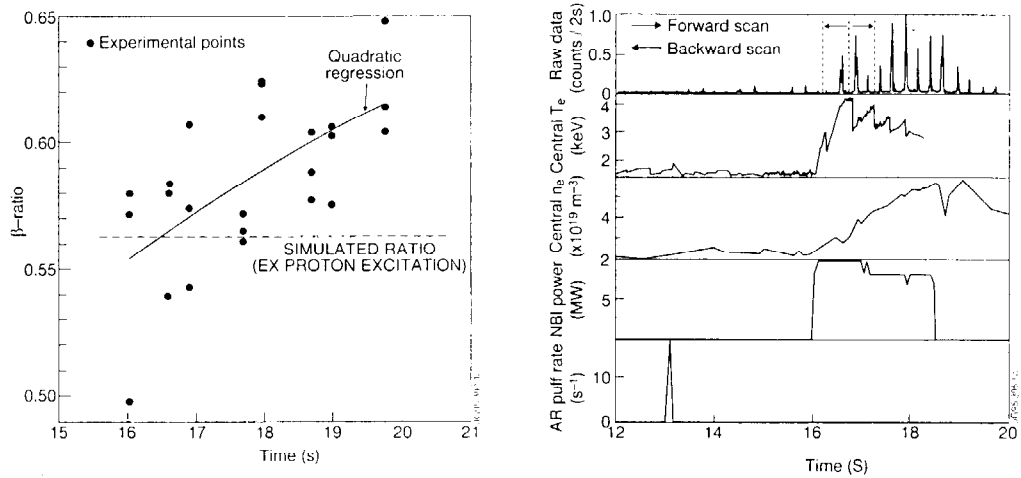
Fig. 4. (Left) Plasma parameters for JPN 23347 (from top): Spectrometer raw data displaying repetitive scans over the Ar XVIII Ly_α components and the He-like Cl XVI n=3 system, T_e (central value, keV) n_e (central value, $\times 10^{13} cm^{-3}$, NBI power (MW), LHCD power (MW) and the argon gas puff rate. JPN's 23345 and 23346 have almost identical parameters. (Right) The measured β-ratio for three JET pulses (JPN's 23345, 23346, 23347) as a function of time (points) The solid curve is a quadratic regression through the measured points. Also shown (dashed line) is the calculated ratio which utilises e^- excitation rates and recombination rates but neglects proton excitation.

6. Conclusions

Unexpectedly high results are found for the Ar G ratio. Atomic radiative and dielectronic recombination rates are thought to be responsible. The reasons behind two distinct regions of experimental ratios must be more rigorously investigated. Good agreement between measured and calculated ratios is found for the α-ratio. In this case, recombination from Ar XVIII to Ar XVII is less significant than for the G ratio but may still be partly responsible for the consistantly higher values of the calculated ratio. The β-ratio agrees qualitatively with theory in that a measurable increase is observed as the density increases by a factor of ~ 3. Proton rates and more elaborate satellite data should be included in future calculations.

7. References

1. Barnsley R 1993 *PhD Thesis* University of Leicester.
2. Coffey I H 1993 *PhD Thesis* Queens University Belfast
3. Gabriel A H 1972 *Mon. R. Astron. Soc.* **160** 99.
4. Lauro-Taroni L 1995 *private communication* Jet Laboratory.
5. Phillips K J H Keenan F P Harra L K McCann S Rachlew-Kallne E Rice J E and Wilson M 1994 *J. Phys. B: At. Mol. Opt. Phys.* **27** 1939.
6. Singleton M 1995 *private communication* Culham Laboratory.
7. Summers H P *Atomic Data and Analysis Structure: User Manual* **JET-IR(94)06**.

ANALYSIS OF EMISSION SPECTRA FROM MARFES IN JET

M G O'Mullane[1], I H Coffey[2], N J Peacock[3], R Giannella, R Reichle
JET Joint Undertaking, Abingdon, Oxon., OX14 3EA, UK
[1] *University College Cork, Ireland,* [2] *Queens University Belfast, Northern Ireland,*
[3] *UKAEA (Government Division) Fusion, Culham Laboratory, Abingdon Oxon., UK*

Abstract

The emission spectra from MARFES (Multifaceted Asymmetric Radiation From the Edge) is examined. These condensation phenomena occur in tokamak plasmas and are toroidally symmetric but have poloidal asymmetry. Emission spectra, from XUV and VUV instruments on JET (Joint European Torus), are analysed to deduce the parameters of a typical MARFE. All atomic data and modelling codes form part of the ADAS system [1] at JET.

1. Introduction

Condensation phenomena are well-known in astrophysical plasmas; e.g. solar prominences [2]. In tokamak plasmas a radiative condensation can result in a localised region of edge plasma becoming cooler and denser than the surrounding background plasma yet remaining in pressure balance [3]. A trigger event, such as a local influx of neutral fuel ions or an MHD instability can cause this local cooling. One of the unusual properties of MARFEs is that while they are toroidally symmetric they do not follow the magnetic field lines and are poloidally asymmetric. The toroidal symmetry is an assumption of most models and wide angle views of the plasma tend to confirm this hypothesis.

MARFES are usually located near the inner wall on the high field side of the torus. Their position is determined by the ion ∇B drift. The MARFE region can remain stationary for $1-2s$ or can oscillate poloidally at frequencies of 20Hz. Figure 1 shows the location of a typical MARFE with the viewing lines of the XUV and VUV spectrometers available at JET. The size has been inferred from a multi-cord bolometer which views the inner wall.

A related phenomenon is the X-point (or 'divertor') MARFE. During radiative divertor experiments nitrogen (or neon) is puffed into the divertor to cause the plasma to detach from the target plates. Large amounts of power (up to 80% of input power) are radiated in $\sim 10\%$ equivalent plasma volume. There are large temperature and density gradients
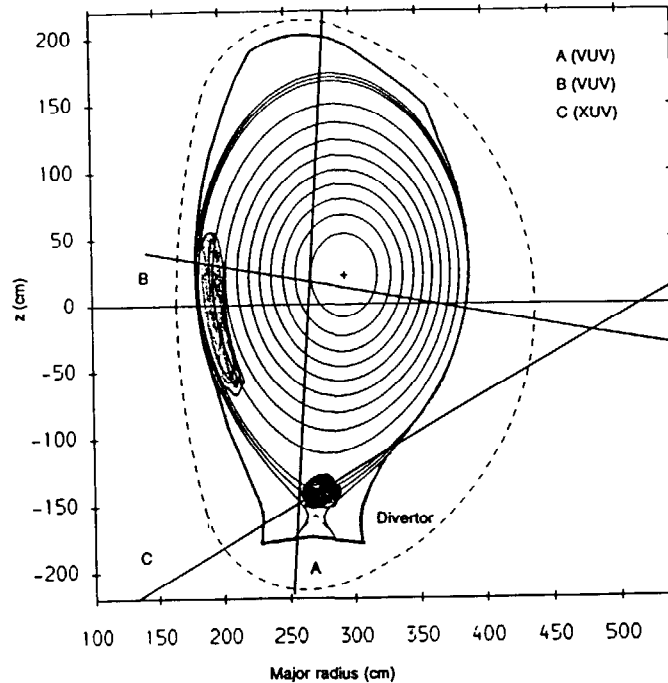
Fig. 1. Poloidal cross-section of JET with magnetic flux surfaces. Also shown are the lines-of-sight of the XUV (Schwob) and VUV (SPRED) spectrometers in JET. The locations of the inner wall MARFE and divertor MARFE are shaded.

parallel to the magnetic field which are ideal conditions for MARFE formation. Following detachment a region of strong emission is observed near the X-point inside the separatrix. The emission region remains stable for 1 − 2s. This is the 'divertor' MARFE.

2. Model of Impurities in a MARFE

The MARFE is sustained by the balance between parallel heat conduction from the surrounding plasma and local radiation losses. When the radiation exceeds the heat inflow and $\partial P_{rad}/\partial T_e$ of impurity radiation is at a minimum the MARFE forms. Low temperatures near the plasma edge and the shape of the impurity radiation curves (P_{rad}) ensure that low Z elements are the causal impurities in MARFE formation at temperatures of $\sim$ 15eV.

Two sources of impurities can give rise to MARFE radiation viz. existing bulk impurities streaming through the MARFE along the field lines and influxes of fresh impurities from the vessel wall. The initial distribution of ionisation stages reflects the origin of the sources (i.e. neutral or reflecting the local diffusive ionisation balance of $T_e \geq$ 100eV). The MARFE alters the edge conditions but the radial distribution of impurity ionisation stages is not significantly affected since the re-ionisation time of a particle leaving the MARFE is shorter than its transit time around the torus. The time taken for incoming ions to attain MARFE temperatures, the thermalisation time, is $\sim 10^{-7}$s, faster than atomic processes. The subsequent evolution of the impurities in the MARFE is determined by their residence time and the atomic timescales. Populations of ionisation stages

14

out of coronal equilibrium are given by the set of coupled equations ($i = 1, Z$)

$$\frac{\partial n_z}{\partial t} + \nabla \cdot \Gamma_z = n_e \left[-n_z S_z + n_{z-1} S_{z-1} - n_z \alpha_z + n_{z+1} \alpha_{z+1} \right] \tag{1}$$

where S_z and α_z are ionisation and recombination coefficients.

The passage of impurities through the MARFE depends on the collisional regime they encounter. The frictional slowing down time ($\tau_\parallel$) determines their motion along the field lines and modifies their parallel velocities from $\frac{1}{3} v_{\text{thermal}}$. The diffusive deflection time ($\tau_\perp$) governs the motion perpendicular to the flux surfaces. Over a range of MARFE temperatures and densities these times are comparable and of the order of a few milliseconds. This is also the timescale to establish ionisation equilibrium in the MARFE. The residence time is estimated at $\sim$ 10ms. The solution of (1) is simplified by replacing the transport term ($\nabla \cdot \Gamma_z$) by (n_z/τ_p) with a confinement time (τ_p) common to all ionisation stages.

The emission in a particular spectrum line is composed of separate independent parts driven by excitation, recombination and possibly charge exchange. The emission from these processes is calculated using ADAS. The total line emission is constructed from these and the time varying ionisation balance.
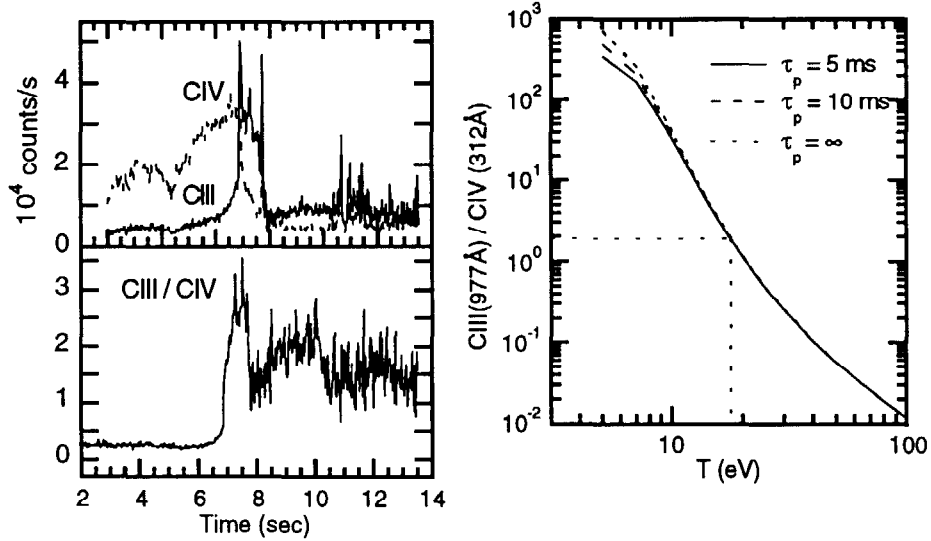

Fig. 2. Variation of CIII, CIV and their ratio (left) during an inner wall MARFE from spectrometer B. The MARFE appears at 6.7s. The calculated ratio is also shown (right) for a 10ms residence time. The dotted line indicates a ratio of 2.0

3. Plasma Parameters of Inner Wall MARFE

Inner wall MARFES form during the limiter phase of the discharge when there is no stabilising divertor. They are characterised by a sharp rise in radiation which usually exceeds the input power. Following some trigger (an influx from plasma-wall interaction) the total radiation increases and becomes localised, as a MARFE, on the inner wall. The localised radiation is accompanied by enhanced deuterium Lymann α (D_α) indicating

15

cooler temperatures. During the MARFE charge exchange features between incoming bare ions and deuterium (e.g. C^{6+}, $n = 4 - 3$ line at 521Å) have been observed.

The inner wall MARFE occasionally lies along the line-of-sight of spectrometer 'B'. Figure 2 shows that the CIV $1s^22s\,{}^2S - 1s^23p\,{}^2P$ 312.4Å line falls with a simultaneous rise in the CIII $2s^2\,{}^1S_0 - 2s2p\,{}^1P_1$ 977Å line indicating that this emission comes from recombining carbon. The transient model, described in section 2, is used to interpret this ratio since these lines are from adjacent ionisation stages. Calculations show that this line ratio is sensitive to temperature. This recombining model suggests that the MARFE temperature is $\sim 16-18$eV. Calculated ratios corresponding to the observed value do not vary greatly with integration time indicating that the carbon has attained near ionisation equilibrium values in the MARFE. The sensitivity of this ratio on confinement time (τ_p) and density is most marked at temperatures below 12eV and can be neglected in this analysis.
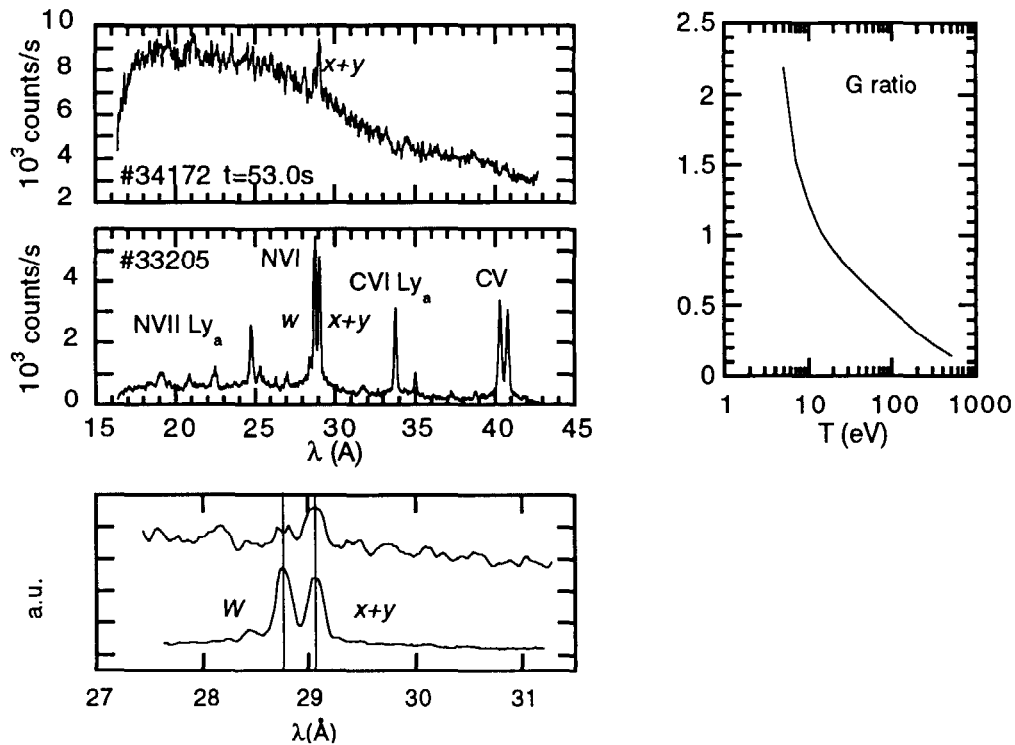

Fig. 3. NVI and NVII in a 'divertor' MARFE discharge (top left) compared to standard nitrogen emission (middle left) in the absence of a MARFE. The NVI shown in greater detail (bottom left). The Nitrogen G ratio in coronal balance is also shown (right).

4. Plasma Parameters of X-point MARFE

The divertor region is monitored by spectrometers 'A' (VUV) and 'C' (XUV) with intersecting lines-of-sight which together give spectral coverage of NII-NVII. When nitrogen is puffed the nitrogen radiation swamps the intrinsic carbon. In the VUV the dominant ionisation stages are NIV and NV with NIII rising throughout the gas puffing phase. The ionisation balance temperatures is ~ 20eV.

The XUV spectrometer shows no evidence of strong radiation from H- and He-like

nitrogen during the radiative divertor phase. The NVI intercombination line becomes the strongest NVI line indicative of a strongly recombining plasma. The expanded NVI spectrum of figure 3 (bottom left) shows the absence of the resonance line. The calculated G ratio (intercombination $(1s^2\,^1S_0 - 1s2p\,^3P_1)$ / resonance $(1s^2\,^1S_0 - 1s2p\,^1P_1)$; $x + y/w$) in coronal equilibrium indicates that a large G ratio is a measure of low electron temperature. Irrespective of the equilibrium conditions the 'observed' G ratio indicates very cold temperatures of less than 10eV in the X-point MARFE.

5. Discussion and Conclusions

It remains to directly measure the temperature and density of a MARFE simultaneously. MARFES are in pressure balance. Appropriate diagnostics are required to test whether there is a concomitant rise in density. The toroidal symmetry also remains to be confirmed experimentally. Streaming particles through the MARFE will leave a recombination dominated spectrum. A contiguous spectral coverage $(5 - 3000\text{Å}$ perhaps?) is necessary to reconcile the fragmentary observations with such theories.

XUV and VUV observations of MARFES have been interpreted and suggest electron temperatures of 16eV for inner wall MARFES with somewhat lower temperatures for the divertor MARFE. Transport within the MARFE is different from that of the surrounding plasma and the collisionality may be high enough to retain impurities for a sufficient time for them to attain ionisation equilibrium.

Acknowledgements

1. Summers, H. P., 1994, *The Atomic Data and Analysis Structure (ADAS) User Manual* JET Internal Report, JET-IR(94)06
2. Parker, E. N., 1953, *Astrophys. J.* **117** 431.
3. Lipschultz, B., 1987, *J. Nucl. Mater.* **145–147** 15.